RSC Advances

ROYAL SOCIETY OF CHEMISTRY

www.rsc.org/advances

Morphological changes in carbon nanohorns under stress: a combined Raman spectroscopy and TEM study

Miriam Peña-Álvarez[a], Elena del Corro[a,b], Fernando Langa[c], Valentín G. Baonza[a], Mercedes Taravillo[a*]

[a]MALTA-Consolider Team, Department of Physical Chemistry I, Chemistry Faculty, University Complutense of Madrid, 28040 Madrid, Spain

[b]J. Heyrovsky Institute of Physical Chemistry of the Academy of Sciences of the Czech Republic, v.v.i., Dolejskova 3, 182 23 Prague 8, Czech Republic

[c]University of Castilla-La Mancha, Instituto de Nanociencia, Nanotecnología y Materiales Moleculares (INAMOL), 45071, Toledo, Spain

[*]mtaravil@ucm.es

ABSTRACT

In this work, we present the first study of highly compressed carbon nanohorns (CNHs). The experiments were performed in a sapphire anvil cell and the morphological changes induced in the CNHs samples were monitored simultaneously by Raman spectroscopy and subsequently by Transmission Electron Microscopy. CNHs samples subjected to a maximum stress of 8 GPa in a single direct compression cycle showed broadened Raman spectra, corresponding to carbonaceous regions with graphite-like structures, surrounded by debundled dahlias-like structures. However, samples subjected to a moderate stress single cycle (2 GPa) exhibit morphological changes from dahlia-like to bud-like structures. Finally, consecutive moderate stress cycles leads to the aggregation of such bud spheres towards the formation of a laminar material with horns-like structures at the edges; a very promising configuration for targeted functionalization. This study demonstrates the advantages of using stress for pretreating CNHs samples for subsequent reactivity and functionalization studies.

INTRODUCTION

Since the discovery of carbon nanotubes (CNTs) in 1991,[1] much research has been done to develop more efficient and cleaner synthetic routes. In 1999, Ijima *et al*., synthesized for the first time a related material: single walled carbon nanohorns (SWCNHs) which can be now obtained without the need of any catalyst.[2] This fact turns this new material into an excellent candidate to work with clean and pure carbon materials, so overcoming some of the CNTs disadvantages. SWCNHs are single graphitic sheets wrapped into nano-sized tubules of 2-3 nm diameter, closed with cone caps of average cone angel ~20º. Their tubular shape, together with their cone tip, provides CNHs a selective reactivity towards either the tip or the tube walls, connecting each region to certain functional groups. One key advantage is that, combined with other carbon materials such as fullerenes, functionalization reactions can be conducted in solution under mild conditions, in contrast to what occurs in CNTs.[3] Depending on the conditions under which they were produced, SWCNHs aggregate with different shapes; four different types have been identified: dahlia-like, bud-like, seed-like and petal-like.

CNTs are very stiff materials, with Young modulus of about 1 TPa,[4,5] whose response to high pressure has been already explored.[6,7] Concerning morphological changes under stress, first, along their radial direction, CNTs collapse at certain pressure values, depending on their diameter and number of walls;[8-12] and second, high stress provides a mechanical alternative to debundle CNTs.[6] So far, little is known about the response of CNHs to stress and possible debundling effects. Just, a few previous works[13,14] showed how repeated hydrostatic compressions of SWCNHs up to 50 MPa, generated high bulk density nanocarbon material which could be used as methane storage with high capacity; due to the generation of two type of channels with different geometry, intratubular and interstitial.

As in other graphitic materials, Raman spectroscopy is among the best diagnostic tools for providing information about the mechanical properties,[7,15,16,17] and the stress induced morphological changes.[13] Additionally, molecular dynamics[18,19,20] studies carried out on graphene, have demonstrated how the mechanical properties of a graphene layer strongly depend on its morphology and defects distribution. The Raman spectra of CNHs appear quite similar to those of their CNTs analogues, but showing broader features. Due to their conical shape, CNHs present larger diameter distribution which implies a wider G band distribution;[21] and the coexistence of pentagonal and heptagonal rings into the hexagonal carbon network also justifies the observed broadening of the D band.[22] However, in contrast to what is observed in the Raman spectra of CNTs,[23] radial breathing modes are absent in CNHs, probably because of their distorted symmetry.

In this work, we study the changes induced by stress in several CNHs samples by combining in-situ Raman spectroscopy and Transmission Electronic Microscopy (TEM) on the recovered samples. We observe that the application of a single high stress cycle generates carbonaceous regions with graphite like structure, within a sample with broken dahlias morphology. However, after consecutive moderate stress-cycles over the same CNHs sample, a layered material with graphite-like surfaces and horns remaining on the edges is formed. These observations provide an important reference for characterizing CNHs in future applications and open new avenues for stress-controlled pretreatment of CNHs that may develop into tailored and targeted functionalization reactions.

MATERIALS AND METHODS

In this work we use dahlia-like aggregates of CNHs of 90% purity. They were produced by CO_2 laser ablation of graphite in the absence of any metal catalyst under an argon atmosphere (760 Torr) at room temperature, as described elsewhere.[2]

Raman spectroscopy. Two Raman setups were used in this work. The first is based on an ISA HR460 monochromator using a 600 grooves·mm^{-1} grating and liquid nitrogen cooled CCD detector (ISA CCD3000, 1024×256 pixels). The sample was excited at 532 nm using a Spectra Physics solid-state laser and the scattered light was collected using a 10x Mitutoyo long-working distance objective coupled to a 10x Navitar zoom. The second Raman setup is a confocal BWTEK Voyage™ BWS435-532SY spectrometer coupled to an Olympus BX51 microscope; we used a 532.0 nm solid-state laser as excitation line and a 20x long-working distance microscope objective. The CCD detector is based on a 2048×122 pixels back-thinned Hamamatsu S10141-1107S chip, thermoelectrically cooled to 253 K. All the spectra were excited at laser powers of about 0.16 mW to avoid sample heating and damaging. Typical sampling areas were about 1-2 μm in diameter. Spectra were measured at spectral resolutions of about 2-3 cm^{-1} and calibrated with a standard Ne-emission lamp.

TEM characterization. Recovered specimens after stress were analyzed with a transmission electron microscope (JEOL JEM 2100 operated at 200 kV), and a high resolution transmission electron microscope (JEOL JEM-3000F, operated at 300 kV) from the spanish CNME facility.[24]

High stress experiments. These experiments were conducted using a Sapphire Anvil Cell (SAC) described elsewhere.[25] The CNHs samples were supported on Inconel gaskets (not drilled), so that after the stress treatment the samples could be recovered to perform successful TEM experiments. Using this configuration non-hydrostatic stresses are generated and unwanted interactions between pressure-transmitting media and the CNHs samples are discarded. This configuration requires using the Raman shifts of the sapphire anvil bands (A_{1g} and E_g modes at 417 and 750 cm^{-1}, respectively[26,27]) as secondary standards to estimate the local effective stress, σ_{eff}, acting on the sample.[28,29] Two kinds of stress experiments were

performed. First, a single stress cycle up to 8 GPa was applied on a given sample, in which Raman spectra were collected at increasing small stress steps. Second, consecutive lower stress cycles (2 GPa, 20 cycles maximum) were applied over CNHs samples and Raman spectra were registered at the maximum stress and on the recovered sample). Both kinds of experiments were run at least two times to confirm the reproducibility of the measurements.

RESULTS AND DISCUSSION

In Figure 1 we present the Raman spectrum of pristine SWCNHs at room conditions. It exhibits the typical sp^2 defected carbon materials first-order features: the D (~1350 cm^{-1}) and the G (~1589 cm^{-1}) bands.[30,31] In CNHs the D band is originated from two kind of topological distortions relative to a perfect sp^2 graphene hexagonal lattice: 1) layer folding, similar to a armchair-like edge in CNTs,[32] and 2) pentagons to generate the characteristic conical-like shape and the CNH's apex.[22] The later topological D band appears about 50 cm^{-1} downshifted from the usually present D band;[22] thus deriving, at low resolution conditions, in a unresolved broad (Full Width at Half Maximum (FWHM) ~ 60 cm^{-1}) D band. The G band also presents a FWHM (*ca.* 55 cm^{-1}) larger than graphite and graphene at room conditions[33,34] and it is centered at a slightly higher frequency.[31] Such differences with respect to other pristine sp^2 carbon materials,[35] can be very likely attributed to remaining amorphous carbon (a-C) resulting from the CNHs synthesis. In fact, CNHs have a small percentage of a-C, which shows a G band around 1510 cm^{-1},[30,31,36] that contributes to additional broadening in both G and D profiles. The Raman spectrum of a-C also presents less intense Raman features around 1350 and 2750 cm^{-1},[37] that cannot be distinguished in the spectrum of pristine CNHs but that may appear under compression. CNHs' first-order spectrum is also formed by the D' band, around 1615 cm^{-1}, as a shoulder of the G band,[15] with an intensity proportional to that of the D band.[38] Regarding the second-order Raman spectra, the most intense contribution is

the characteristic 2D band (2678 cm^{-1}), which varies with the ABAB stacking of graphene layers in graphite[39] and the graphitic crystal size.[40] Additional Raman contributions like the D+D´´ band (2451 cm^{-1}) and the D+D´ band (2799 cm^{-1}),[41] which are also activated by disorder and showing intensities proportional to that of the D band, are observed in the Raman spectra of compressed CNHs.

Morphological changes under high stress

Figure 2 shows the evolution of the Raman spectrum of CNHs with increasing stress. As expected from previous carbon materials studies,[6,34] a general upshift with stress is observed. As already commented in the introduction, CNTs under compression undergo a flattening of their circular section[8,9,10] at a stress threshold that varies depending on the diameter and the number of walls in the tube.[11,12] Specifically, the flattening stress barrier is lower for single-walled tubes with larger diameter (0.8 GPa for 1.6 nm diameter tubes).[8] Therefore, we may expect flattening of the horns in our CNHs samples (2-3 nm) at stresses below 0.5 GPa; this provides a stress limit beyond which additional compression would lead to the formation of graphite-like carbon.[42] Unfortunately, the stress value estimated for a similar transition in CNHs is below the detection limit in our experimental setup, and the evolution of the Raman frequencies with stress follows a linear behavior over the whole stress range monitored in this work. Moreover, the Raman spectrum of the recovered sample is presented in red in Figure 2; it shows an upshift of the main Raman features, giving a clear indication of a debundling process of the CNHs sample, similar to that already described in the literature for CNTs[6] and confirmed by the TEM images discussed below.

An increase of the stress on the sample induces a broadening of the whole Raman spectrum. From a spectral profile analysis using Lorentzian contributions, we estimate that such broadening is more than 3 times larger for the D band than for the other first-order bands (G

and D'), see Figure 3a. On the other hand, a considerable broadening of the second-order spectrum occurs with increasing stress, and above *ca.* 6 GPa an unexpected vanishing of this spectral range takes place. As mentioned above, a-C presents broad contributions overlapping with the D, 2D and D+D' bands of carbon materials,[37] which are not visible in the Raman spectrum of pristine CNHs but may become more intense with the stress treatment, thus causing the broadening of the spectrum in the corresponding spectral regions. Moreover, vanishing of the combination bands and overtones is also characteristic of the formation of amorphous carbon material, so our findings are indicative of a drastic morphological transition in the compressed sample.

The evolution of the intensity of the Raman bands induced by the stress is plotted in Figures 3b-c, related to the G band intensity. With stress the intensity of the D' band and the G band of a-C increases, a fact that at a first view could be simply related with an increasing generation of defects towards the sample destruction. However, interestingly, the D band decreases in intensity to become approximately equal to that of the G band, thus discarding this possibility. The intensity ratio G/D has been related with the relative amount of double (C=C) and single (C-C) bonds. In other words, such ratio establishes some sort of hybridization scale for the material under study, being infinite for HOPG graphite and zero for diamond.[43, 44] Our results reveal an increase in C=C bonds when the CNHs samples are subjected to large compression. Having into account the evolution with stress of the Raman spectra, as measured by the FWHMs and relative band intensities, we conclude that CNHs turn into a carbonaceous sp^2 structure upon compression. Such modification appears to be only partially reversible, since the intensity of the second-order Raman spectrum after releasing the stress is not fully recovered.

To give additional support to this conclusion we conducted series of TEM experiments on the recovered samples. In Figures 4 and 5 we show selected TEM images (under different

magnifications) of both pristine CNHs and the corresponding recovered sample after an 8 GPa stress cycle, respectively. The TEM images of the pristine sample correspond to CNHs aggregates exhibiting dahlia-like morphology.[45] The TEM images of the recovered samples resembles that of amorphous carbon (Figure 5a-b) at low resolution, but at the highest magnification a clear graphitic-like structure is distinguished (Figure 5c). Furthermore, a remarkable observation is that while the interlayer spacing between single CNHs is about 0.4 nm in pristine CNHs, which is 18% larger than that of graphite,[46,47] the interlayer distance deduced from Figure 5c is closer to 0.34 nm, which exactly corresponds to the typical van der Waals interlayer distance in graphite. This observation justifies the relative increase observed in the I_G/I_D ratio deduced from the Raman spectra. In other regions of the recovered sample (Figure 5d-f) we observe that the CNHs still remain as aggregates, but they have lost their initial dahlia-like shape. These regions consist of aggregates of debundled CNHs, in good agreement with the remaining upshift observed in the Raman spectrum of the recovered sample (notice that the aggregates have some of their original arrangement, and there are more individual horns which look more parallel to each other).[48] Both kind of TEM images, those corresponding to sp^2 amorphous carbon and those to debundled aggregates, confirms our previous discussion on the Raman spectrum of the recovered samples (bottom red spectrum in Figure 2): the G band of amorphous sp^2 carbon contributes, but the G band of the CNHs still predominates.

Thus, the application of stress promotes a morphological change in CNHs that generates carbonaceous regions with graphite like structure within regions of broken dahlia-like morphology. We believe that these two different responses to stress depending on the region are simply due to different CNHs concentrations in the sample. When the CNHs sample is low concentrated and has the purest quality (low a-C content), the applied stress is essentially invested in debundling the dahlia-like structures; however, in more concentrated samples,

with larger amount of a-C, the formation of graphite like lumps upon stress is observed, as if a-C were acting as a seed for generating such kind of morphology.

Moderate compression/decompression cycles on CNHs

We also subjected different CNHs samples to several moderate-stress cycles (maximum stress ~2 GPa), in order to analyze a possible high bulk density material formation like that obtained by other authors elsewhere,[13,14] after consecutive 50 MPa hydrostatic pressure cycles. In Figure 6 we compare the Raman spectra of the recovered samples after consecutive compression-decompression cycles with the Raman spectrum of pristine CNHs. In contrast to the increase in the a-C content observed after a higher stress treatment, when the samples are subjected to several moderate-stress cycles the graphitic crystallinity remains, as proven by the Raman spectra of the recovered sample where the second order features remain visible and the G band of the amorphous carbon does not increase. In contrast with the observations of Bekyarova *et al.*,[13,14] broadening of the Raman spectrum is barely observed; furthermore, we see in Figure 7a that the FWHM of the G band remains almost unaltered after the stress cycles (in fact, it is slightly narrowed). Moreover, the FWHM of the D band also narrows in about 30 cm^{-1}, with respect to that of pristine CNHs, in a sample recovered after 20 stress cycles. This result, together with the slight narrowing of the G band, is indicative of the disappearance of the pentagonal defects and the conical shapes contributions to the spectrum; a conclusion also confirmed by TEM experiments, as will be discussed below. Additionally we observe in Figure 7b that the frequency of the G band of CNHs decreases in about 10 wavenumbers upon stress cycling, approaching the reference value of the G band of highly oriented pyrolytic graphite (HOPG).[33,49] Regarding the intensities variations we observe in Figure 7c that the ratio I_G/I_D decreases from 0.85 to 0.60 after consecutive stress cycles, thus

indicating significant changes in the ratio double (C=C) to single (C-C) bonding in the sample.[43,44]

The above findings are supported by the TEM and HRTEM images of the recovered samples shown in Figure 8. After one stress cycle, a transition from dahlia-like to bud-like carbon nanohorns takes place (Figure 8a-e).[45,49] In this new morphology the horns do not protrude out from aggregates' surface, in contrast to what occurs in the dahlia-like arrangement. Samples consisting of variable CNHs concentrations were subjected to a single stress cycle, and in all cases a certain amount of isolated bud-like aggregates appeared, more extensively in low-concentrated CNHs samples. Thus, it seems that for a single moderate stress cycle bud-like aggregates tend to isolate instead of forming larger protuberances. However, after several consecutive stress cycles (up to six) we observed that the bud-like spheres tend to aggregate (Figure 8f-h) towards the creation of graphite-like surfaces with horns at the edges (Figure 8i-l). After six or more stress cycles, we observe the formation of a layered material (Figures 8m-o), similar to that obtained after a high temperature treatment of CNHs,[49] but with a larger degree of disorder.

CONCLUSIONS

SWCNHs samples have been subjected to several high stress treatments and characterized by combined TEM and Raman spectroscopy in order to evaluate morphological changes upon compression. After a single high stress cycle of ~8 GPa, we observed the appearance of two different formations depending on the initial quantity of CNHs in the pristine sample: debundled dahlias and graphite like lumps (turning into amorphous sp^2 carbon). In contrast, after single lower stress cycle of ~2 GPa the transition from dahlia to bud-like sphere is

observed. Consecutive 2 GPa cycles leads to the aggregation of the bud-like spheres towards the formation of a layered material (with sp^2 graphitic crystallinity) in whose edges, remnant horn structures can be found. All these findings demonstrate the advantages of using high to moderate stress for pretreating CNHs samples, thus increasing their subsequent reactivity and, moreover, opening new possibilities for a tailored and targeted functionalization. Finally, it would be interesting to study the effect of such treatments in their electronic properties.

ACKNOWLEDGEMENTS

We thank Prof. Masako Yudasaka from Nanotube Research Center, National Institute of Advanced Industrial and Technology, Higashi, Japan for a critical reading of the manuscript. We also thank Prof. Iijima (Meijo University) for providing us with the Carbon Nanohorn sample. This work has been supported by MINECO through the projects CSD2007-00045, CTQ2012- 38599-C02-02 and CTQ2013-48252-P. We thank the National Center for Electron Microscopy at Universidad Complutense de Madrid for facilities. MPA is grateful to the Spanish Ministerio de Educación, Cultura y Deporte for an FPU grant.

FIGURES AND CAPTIONS

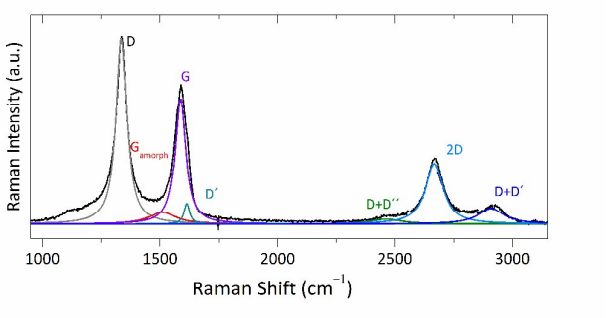

Fig. 1 Raman spectrum of pristine CNHs. Colored lorentzian curves correspond with the different contributions of the spectrum mentioned in the text.

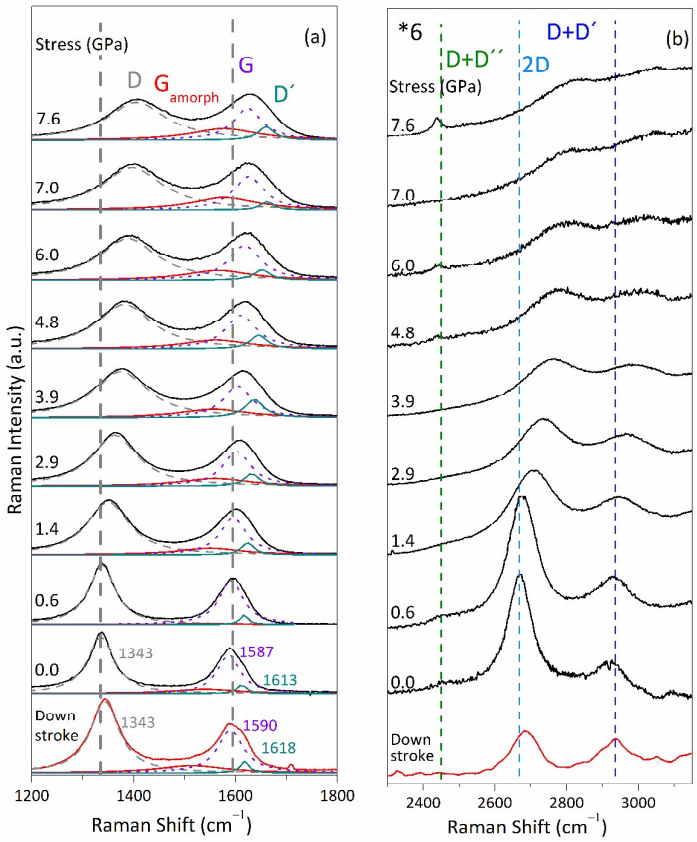

Fig. 2 Raman spectra of CNHs with increasing stress. (a) Fundamental bands in the spectral range 1200-1800 cm^{-1} and (b) combination bands and overtones from 2300 to 3500 cm^{-1}. In (a) the Lorentzian functions representing the most relevant bands are plotted in different colors.

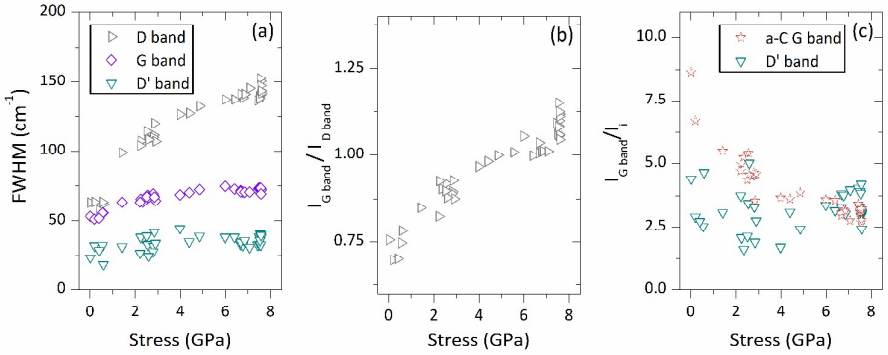

Fig. 3 (a) FWHM of the D, G and D´ bands as a function of applied stress. Intensity ratios (b) I_G/I_D and (c) $I_G/I_{D'}$ and $I_G/I_{a\text{-}CG}$ as a function of stress.

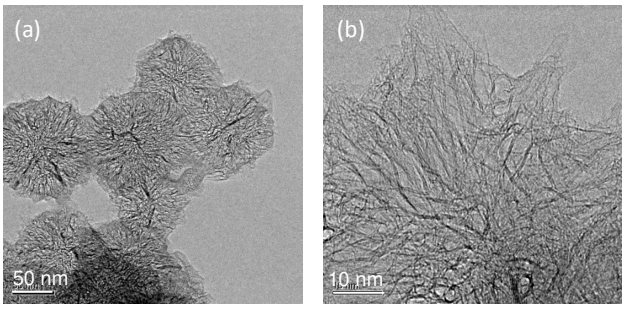

Fig. 4 TEM images of pristine CNHs samples at different magnifications: dahlia-like aggregates.

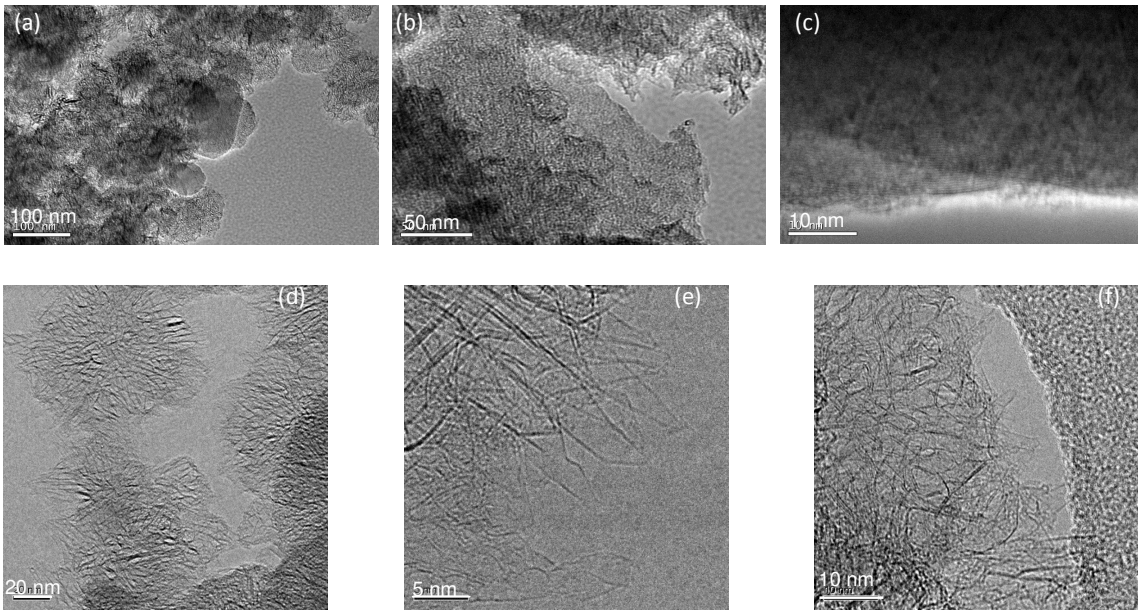

Fig. 5 TEM images at different magnifications of the CNHs sample recovered after a 8 GPa stress cycle, in two different regions, A (a-c) and B (d-f), with graphite-like amorphous carbon and broken dahlias morphologies, respectively.

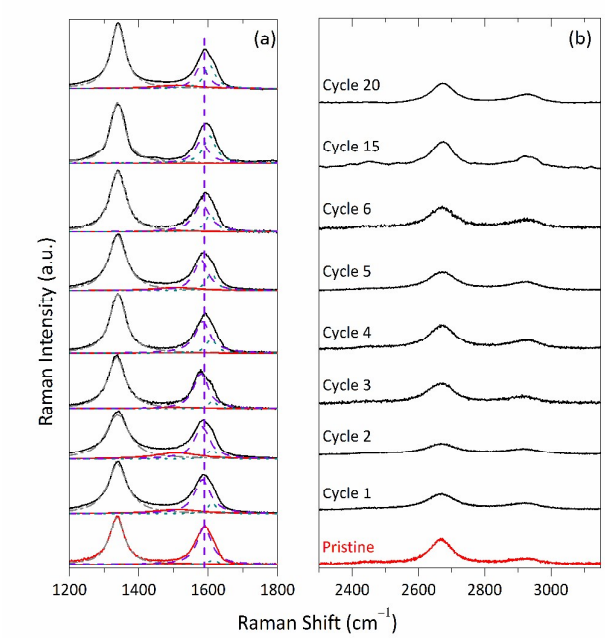

Fig. 6 Raman spectra of a CNHs sample recovered after different consecutive stress cycles up to *ca*. 2 GPa. Labels indicate the maximum cycle number reached for each sample. The red spectrum at the bottom corresponds to that of the pristine CNHs sample.

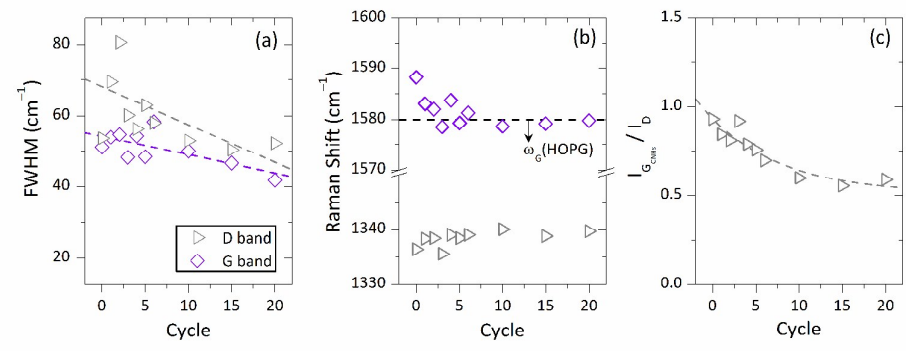

Fig. 7 Characteristics of the D and G bands in recovered CNHs samples as a function of the number of consecutive stress cycles: (a) FWHM, (b) Raman shift and (c) intensity ratio (I_G/I_D).

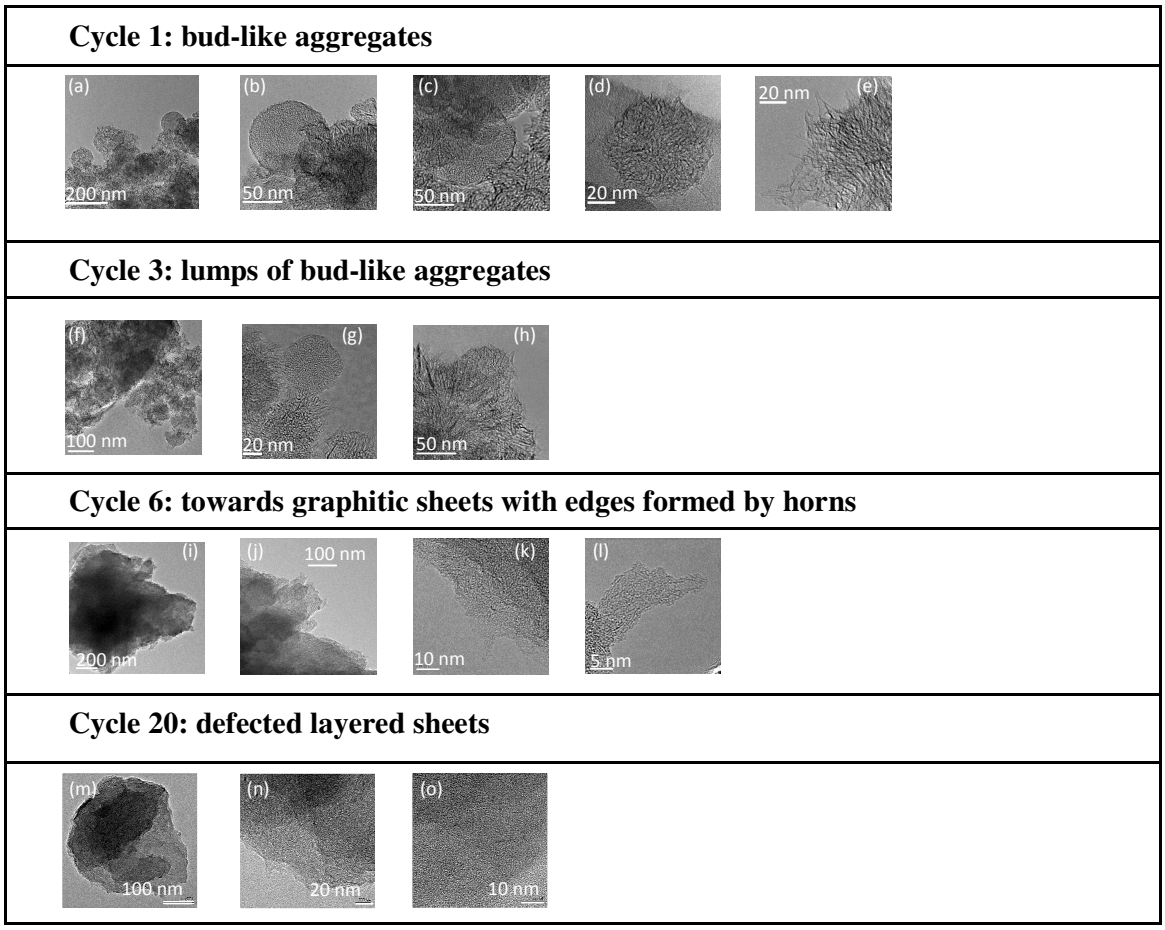

Fig. 8 Selected TEM images of the CNHs samples recovered after a certain number of stress cycles.

REFERENCES

1 S. Iijima, *Nature*, 1991, **354**, 56-58.

2 K. Ajima, M. Yudasaka, K. Suenaga, D. Kasuya, T. Azami and S. Iijima, *Adv. Mater.*, 2004, **16**, 307-401.

3 M. Vizuete, M. J. Gómez-Escalonilla, J. L. G. Fierro, M. Yudasaka, S. Iijima, M. Vartanian, J. Iehl, J. F. Nierengarten and F. Langa, *Chem. Commun*., 2011, **47**, 12771-12773.

4 J. P. Lu, *Phys. Rev. Lett*., 1997, **79**, 1297-1300.

5 M. Meo and M. Rossi, *Comp. Sci. Tech*., 2006, **66**, 1597-1605.

6 E. Del Corro, J. González, M. Taravillo, E. Flahaut and V. G. Baonza, *Nano Lett*., 2008, **8**, 2215-2218.

7 A. J. Ghandour, I. F. Crowe, J. E. Proctor, Y. W. Sun, M. P. Halsall, I. Hernandez, A. Sapelkin and D. J. Dunstan, *Phys. Rev. B*, 2013, **87**, 085416.

8 J. A. Elliott, J. K.W. Sandler, A. H. Windle, R. J. Young and M. S. P. Shaffer, *Phys. Rev. Lett*., 2004, **92**, 095501.

9 D. Y. Sun, D. J. Shu, M. Ji, F. Liu, M. Wang and X. G. Gong, *Phys. Rev. B,* 2004*,* **70**, 165417.

10 M.-F. Yu, T. Kowalewski and R. S. Ruoff, *Phys. Rev. Lett.*, 2001, **86**, 87-90.

11 A. L. Aguiar, A. San-Miguel, E. B. Barros, M. Kalbac, D. Machon, Y. A. Kim, H. Muramatsu, M. Endo and A. G. Souza Filho, *Phys. Rev. B*, 2012, **86**, 195410.

12 A. L. Aguiar, R. B. Capaz, A. G. Souza Filho and A. San-Miguel, *J. Phys. Chem. C,* 2012, **116**, 22637–22645.

13 E. Bekyarova, K. Murata, M. Yudasaka, D. Kasuya, S. Iijima, H. Tanaka, H. Kahoh and Kaneko, *J. Phys. Chem. B,* 2003, **107**, 4681-4684.

14 E. Bekyarova, K. Kaneko, M. Yudasaka, K. Murata, D. Kasuya and S. Iijima, *Adv. Mater*., 2002, **14**, 973-975.

15 M. Peña-Álvarez, E. del Corro, V. G. Baonza and M. Taravillo, *J. Phys. Chem. C*, 2014, **118**, 25132–25140.

16 E. Del Corro, M. Taravillo and V. G. Baonza, *Phys. Rev. B*, 2012, **85**, 033407.

17 U. D. Venkateswaran, A. M. Rao, E. Richter, M. Menon, A. Rinzler, R. E. Smalley and P. C. Eklund, *Phys. Rev. B,* 1999, **59**, 10928-10934.

18 S. Wang, B. Yang, J. Yuan, Y. Si, H. Chen, *Scientific Reports*, 2015, **5**, 14957.

19 B. Yang, S. Wang, Y. Guo, J. Yuan, Y. Si, S. Zhanga, H. Chen, *RSC Adv*., 2014, **4**, 54677-54683.

20 S. Wang, B. Yang, S. Zhang, J. Yuan, Y. Si, H. Chen, *ChemPhysChem*, 2014, **15**, 2749-2755.

21 A. Jorio, A. G. Souza Filho, G. Dresselhaus, M.S. Dresselhaus, A. K. Swan, M.S. Ünlü, B. B. Goldberg, M. A. Pimenta, J. H. Hafner, C. M. Lieber and R. Saito, *Phys. Rev. B*, 2002, **65**, 155412.

22 K. I. Sasaki, Y. Sekine, K. Tateno and H. Gotoh, *Phys. Rev. Lett*., 2013, **111**, 116801.

23 M. S. Dresselhaus, G. Dresselhaus, R. Saito and A. Jorio, *Phys. Reports*, 2005, **409**, 47-99.

24 http://www.cnme.es/

25 V. G. Baonza, M. Taravillo, A. Arencibia, M. Cáceres and J. Núñez, *J. Raman Spectrosc*., 2003, **34**, 264-270.

26 G. H. Watson Jr., W. B. Daniels and C. S. Wang, *J. Appl. Phys*., 1981, **52**, 956-958.

27 J. A. Xu, E. Huang, J. F. Lin and L. Y. Xu, *Amer. Mineral*., 1995, **80**, 1157-1165.

28 P. Loubeyre, F. Occelli and R. LeToullec, *Nature*, 2002, **416**, 613-617.

29 B. J. Baer, M. E. Chang and W. J. Evans, *J. Appl. Phys*., 2008, **104**, 034504.

30 T. Yamaguchi, S. Bandow and S. Iijima, *Chem. Phys. Lett*., 2004, **389**, 181-185.

31 A. C. Ferrari and J. Robertson, *Phys Rev. B*, 2000, **61**, 14095-14107.

32 L. G. Cançado, M. A. Pimenta, B. R. A. Neves, M. S. S Dantas and A. Jorio, *Phys. Rev. Lett*., 2004, **93**, 247201.

33 A. C. Ferrari, J. C. Meyer, V. Scardaci, C. Casiraghi, M. Lazzeri, F. Mauri, S. Piscanec, D. Jiang, K. S. Novoselov, S. Roth and A. K. Geim, *Phys. Rev. Lett*., 2006, **97**, 187401.

34 E. del Corro, A. Otero de la Roza, M. Taravillo and V. G. Baonza, *Carbon*, 2012, **50**, 4600-4606.

35 T. Ch. Hirschmann, P. T. Araujo, H. Muramatsu, J. F. Rodriguez-Nieva, M. Seifert, K. Nielsch, Y. Ahm Kim and M. S. Dresselhaus, *ACS Nano,* 2014, **8**, 1330–1341.

36 R. Saito, A. Jorio, A. G. S. Filho, A. Grueneis, M. A. Pimenta, D. Dresselhaus and M. S. Dresselhaus, *Physica B*, 2002, **323**, 100-106.

37 J. Hong, M. K. Park, E. J. Lee, D. Lee, D. S. Hwang and S. Ryu, *Sci. Rep*., 2013, **3**, 2700.

38 E. Del Corro, M. Taravillo and V. G. Baonza, *J. Raman. Spectrosc*., 2014, **45**, 476-480.

39 N. Larouche and B. L. Stansfield, *Carbon*, 2010, **48**, 620–629.

40 R. J. Nemanich and S. A. Dolin, *Phys. Rev. B*, 1979, **20**, 392–401.

41 A. C. Ferrari and D. M. Basko, *Nature Nanotech*., 2013, **8**, 235-246.

42 F. Colonna, A. Fasolino and E. J. Meijer, *Phys. Rev. B*, 2013, **88**, 165416.

43 S. Utsumi, H. Honda, Y. Hattori, H. Kanoh, K. Takahashi, H. Sakai, M. Abe, M. Yudasaka, S. Iijima and K. Kaneko, *J. Phys. Chem. C*, 2007, **111**, 5572-5575.

44 R. Yuge, S. Bandow, K. Nakahara, M. Yudasaka, K. Toyama, T. Yamaguchi, S. Iijima and T. Manako, *Carbon*, 2014, **75**, 322-326.

45 S. Iijima, M. Yudasaka, R. Yamada, S. Bandow, K. Suenaga, F. Kokai and K. Takahashi, *Chem. Phys. Lett*., 1999, **309**, 165-170.

46 S. Bandow, F. Kokai, K. Takahashi, M. Yudasaka, L. C. Qin and S. Iijima, *Chem. Phys. Lett*., 2000, **321**, 514-519.

47 K. Yoshizawa, T. Yumura, T. Yamabe and S. Bandow, *J. Am. Chem. Soc*. 2000, **122**, 11871-11875.

48 M. Zhang, M. Yudasaka, J. Miyawaki, J. Fan and S. Iijima, *J. Phys. Chem. B,* 2005, **109**, 22201-22204.

49 D. Kasuya, M. Yudasaka, K. Takahashi, F. Kokai and S. Iijima, *J. Phys. Chem. B,* 2002, **106**, 4947-4951.